Earth and Planetary Science Letters, 77 (1986) 203–217
Elsevier Science Publishers B.V., Amsterdam – Printed in The Netherlands

[4]

Evidence of mantle metasomatism and heterogeneity from peridotite inclusions of northeastern Brazil and Paraguay

P. Comin-Chiaramonti [1], G. Demarchi [1], V.A.V. Girardi [2], F. Princivalle [1] and S. Sinigoi [1]

[1] *Istituto di Mineralogia e Petrografia dell'Università, Piazzale Europa, 1, I-34100 Trieste (Italy)*
[2] *Instituto de Geociências, Universidade de São Paulo, USP, C.P. 20899, São Paulo SP (Brazil)*

Received May 12, 1985; revised version accepted December 2, 1985

Textural-petrographic features, major and trace elements and mineral chemistry are reported for spinel-peridotite xenoliths from northeastern Brazil (NE-suite) and Paraguay (PY-suite).
Variation trends defined by bulk rock and mineral chemistry are consistent with the effects of variable degree of high-pressure melting for both suites.
The PY-suite strongly differs from the NE-suite by its very high contents of incompatible elements. This different whole-rock chemistry is related to the presence of glassy-microcrystalline blebs which are interpreted as remains of pre-existing hydrous phases of metasomatic origin. The difference between the two suites is also recorded in the chemistry of pyroxenes and spinels, which develop along different variation patterns.
Although the suites partially overlap in their ranges of mg_{opx} ($Mg/(Fe^{2+}+Fe^{3+})$ ratio in orthopyroxenes), the PY-suite is, on the average, more mg_{opx} rich (residual) than the NE-suite. Within the PY-suite a rough positive correlation exists between degree of residuality and degree of metasomatic effects.
The sharp differences between the NE-suite and the PY-suite imply mantle heterogeneity on regional scale, whereas the variability within each suite is essentially related to different degrees of melting and/or metasomatism and imply mantle heterogeneity on local scale.

1. Introduction

Peridotite nodules enclosed in alkali basalts have been previously noted in some localities of northeastern Brazil and Paraguay [1].

A preliminary sampling has been carried out from some xenolith-rich occurrences in the Rio Grande do Norte State of Brazil (Pico Cabugi, PC; Serra Aguda, SA; Cerro Corà, CC) and in Paraguay, near Asunciòn (Ñemby, Lambarè, Nueva Teblada, Tacumbù).

Xenoliths from northeastern Brazil, hereafter called the NE-suite, are found in fresh lavas occurring in small plugs. The lavas are basanites (PC and SA) or nepheline-normative olivine-rich basalts (CC), which range in age from 18 to 42 m.y. [2]. The nodules range from small dismembered pieces (less than 1 cm) up to 25 cm in diameter, with the highest size frequency around 3–5 cm. Information about the geological setting and petrography of the northeastern Brazil Tertiary basaltic province is given in [3,4].

Xenoliths from Paraguay, hereafter called the PY-suite, are found in Eo-Oligocene nephelinites and are particularly abundant at the Ñemby locality. The size varies from a few centimeters up to 40 cm, with the highest size frequency around 5–7 cm. Further data can be found in [5,6].

All the xenoliths of this study are spinel-peridotites with the typical four-phase assemblage: olivine (ol), orthopyroxene (opx), clinopyroxene (cpx) and spinel (sp) in order of decreasing amount.

Gabbroic nodules and olivine and clinopyroxene megacrysts have also been collected, but are not considered in this study.

The xenolith suites reported in this paper provide information concerning the mantle composition below northeastern Brazil and Paraguay, on which at present there are no data.

2. Petrography

2.1. General textural features

The textural features here outlined are common to all nodules, although they are differently devel-

0012-821X/86/$03.50

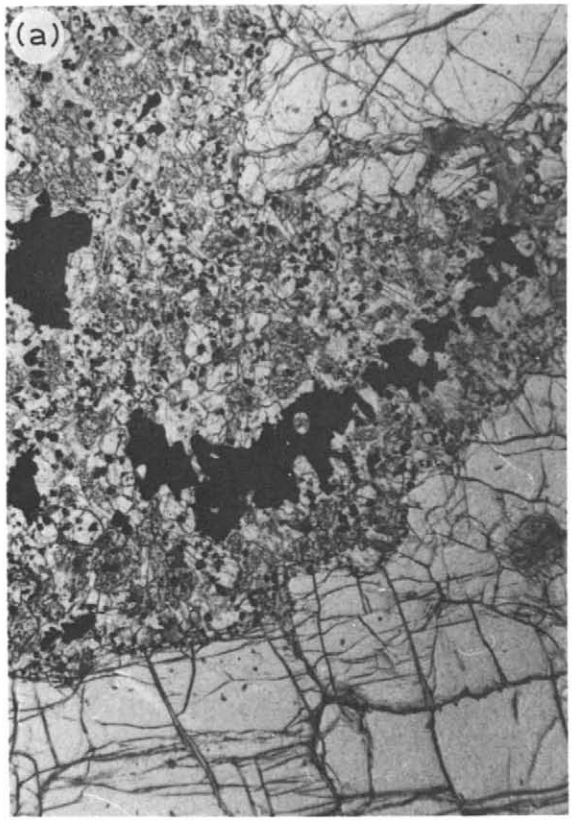
(a)

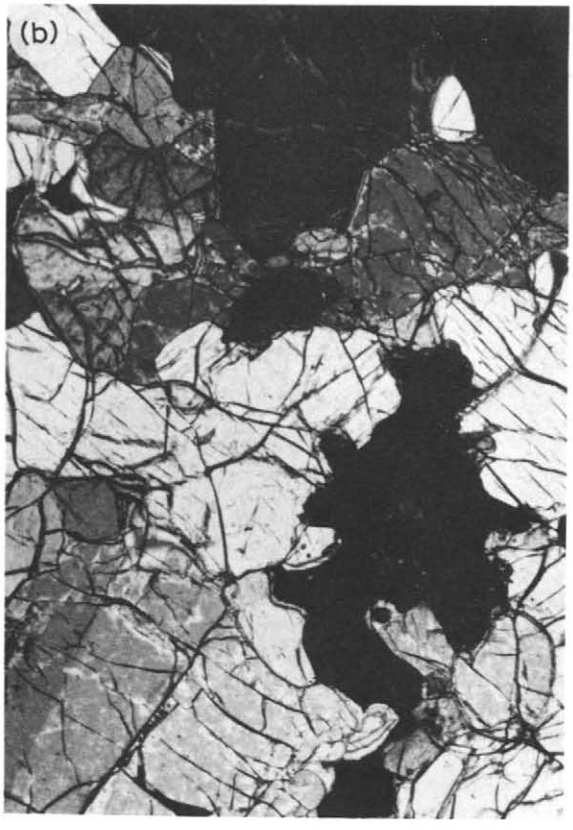
(b)

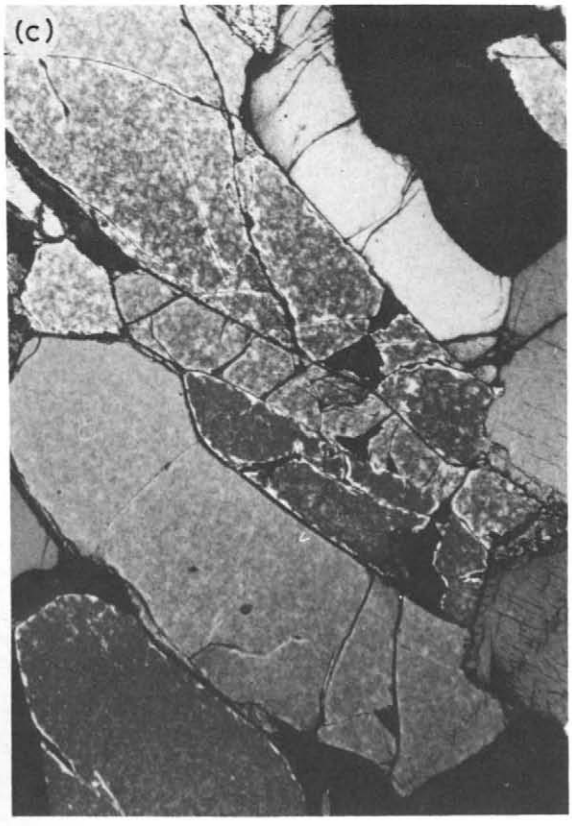
(c)

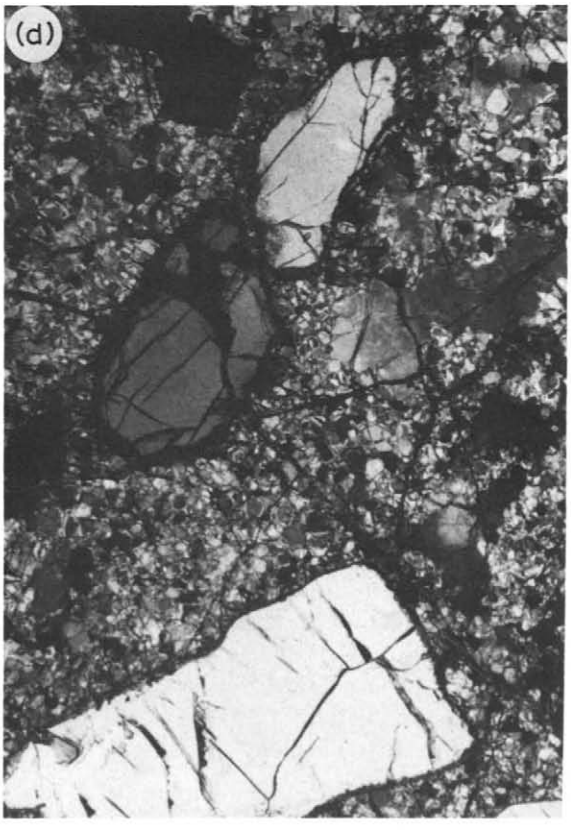
(d)

TABLE 1

Representative microprobe analyses of orthopyroxenes and clinopyroxenes. Cations on the basis of 6 oxygens. Fe^{3+} has been calculated on the charge balance, taking into account the number of cations obtained on the basis of 6 oxygens

	Orthopyroxenes						Clinopyroxenes					
Specimen No.:	1	2	5	7	8	9	1	2	5	7	8	9
Sample	PY3091	PY3092	PY3101	SA23	CC29	CC37	PY3091	PY3092	PY3101	SA23	CC29	CC37
SiO_2	57.25	55.03	55.51	55.14	54.99	53.73	52.95	52.80	53.39	52.09	52.42	51.25
TiO_2	0.08	0.01	0.02	0.12	0.05	0.12	0.24	0.03	0.22	0.43	0.14	0.63
Al_2O_3	1.95	2.39	2.76	3.98	3.15	4.33	2.90	2.83	1.32	5.97	4.23	7.02
FeO_t	5.62	5.41	5.75	5.78	5.58	6.20	2.40	2.13	2.17	2.47	2.17	2.68
MnO	0.15	0.14	0.14	0.14	0.14	0.18	0.00	0.09	0.08	0.08	0.07	0.10
MgO	35.06	35.44	33.93	33.90	34.64	33.16	17.14	17.32	17.64	15.53	16.52	15.19
CaO	0.46	0.39	0.69	0.56	0.54	0.57	19.61	22.66	22.65	20.35	21.97	20.26
Na_2O	0.18	0.02	0.11	0.05	0.04	0.09	1.06	0.58	0.42	1.34	0.92	1.63
Cr_2O_3	0.40	0.36	0.40	0.39	0.46	0.26	2.10	0.73	0.94	1.06	1.09	0.75
SUM	101.15	99.19	99.31	100.07	99.53	98.64	98.42	99.17	98.83	99.32	99.53	99.51
Si	1.9488	1.9130	1.9284	1.9007	1.9053	1.8849	1.9436	1.9316	1.9606	1.8942	1.9094	1.8639
Ti	0.0020	0.0100	0.0005	0.0031	0.0013	0.0032	0.0066	0.0008	0.0061	0.0117	0.0038	0.0172
Al	0.0782	0.0979	0.1130	0.1617	0.1286	0.1790	0.1254	0.1220	0.0571	0.2558	0.1816	0.3008
Al^{IV}	0.0512	0.0870	0.0716	0.0993	0.0947	0.1151	0.0564	0.0684	0.0394	0.1058	0.0906	0.1361
Al^{VI}	0.0270	0.0109	0.0413	0.0624	0.0339	0.0639	0.0690	0.0536	0.0178	0.1500	0.0909	0.1647
Fe^{3+}	0.0315	0.1012	0.0383	0.0356	0.0725	0.0655	0.0000	0.0495	0.0180	0.0000	0.0389	0.0446
Fe^{2+}	0.1284	0.0560	0.1287	0.1310	0.0893	0.1163	0.0736	0.0156	0.0486	0.0751	0.0272	0.0365
Mn	0.0043	0.0041	0.0041	0.0041	0.0041	0.0053	0.0000	0.0028	0.0025	0.0025	0.0022	0.0031
Mg	1.7778	1.8352	1.7558	1.7407	1.7878	1.7328	0.9372	0.9439	0.9649	0.8412	0.8963	0.8229
Ca	0.0168	0.0145	0.0257	0.0207	0.0200	0.0214	0.7710	0.8880	0.8910	0.7927	0.8572	0.7893
Na	0.0119	0.0013	0.0074	0.0033	0.0027	0.0061	0.0754	0.0411	0.0299	0.0944	0.0649	0.1149
Cr	0.0108	0.0099	0.0110	0.0106	0.0126	0.0072	0.0609	0.0211	0.0273	0.0305	0.0314	0.0216

[a] Specimen numbers as given in Table 3.

oped from sample to sample:

(1) Spongy borders are strongly developed in cpx and weakly developed in opx, but absent in ol.

(2) Cr-spinel is mostly interstitial among pyroxenes, with a characteristic "holly-leaf" outline. Spinels found on the border of the xenoliths, in contact with the host lava, show a black oxidation rim.

(3) Sulfides (pyrrhotite and pentlandite) occur in almost all the xenoliths in variable, but small, amounts. They are found as two textural types: (a) as small drops resulting from liquid-exsolution, along the spongy rims of pyroxenes or in glassy patches; (b) associated with fluid inclusions along sealed crystal fractures.

In addition to these features, in general xenoliths from the PY-suite display glassy-microcrystalline blebs and/or interstitial glass. The blebs (Fig. 1a) conform to the description of Maaløe and Prinzlau [7]. They are developed around spinels which display a strongly lobate shape. When the blebs are present, spinels are only found enclosed within them, except for a few, which are enclosed in olivine. The blebs consist of ol, cpx and euhedral Cr-sp microlites in a glassy-feldspathic matrix.

Two kinds of glasses are present: a pale brown glass and a colorless one. They are frequently accompanied by devitrification products. Both blebs and interstitial glasses are generally rounded and separated from each other, and are not aligned along fractures. They are particularly abundant in some larger-sized xenoliths (e.g. samples PY3091, PY3095: diam. 12 cm).

Fig. 1. (a). Glassy-microcrystalline bleb enclosing relict spinels (plain light). (b) Coarse-grained texture. Spinel, usually as interstitial phase, displays a holly-leaf shape (crossed nicols). (c) Tabular texture with undeformed elongated olivine crystals (crossed nicols). (d) Porphyroclastic-mosaic texture showing porphyroclasts of pyroxenes in a fine-grained mosaic of recrystallized olivine (crossed nicols). (Width for all pictures 2.7 mm.)

2.2. Textures

Three main types of textures, apparently related to different degrees of strain and recrystallization, have been identified (nomenclature according to Boullier and Nicolas [8]):

(a) Coarse-grained texture with one generation of crystals with curved borders. This is the dominant textural type and the only one found in the PY-suite (Fig. 1b).

(b) Weakly tabular texture with one generation of crystals. Only two xenoliths display this texture clearly (Fig. 1c).

(c) Porphyroclastic-mosaic texture, which is characterized by shear and recrystallization features, with two generations of crystals. Only four xenoliths display this texture (Fig. 1d).

Some nodules exhibit textures intermediate between the ones mentioned above.

On the basis of textural features, the nodules from northeastern Brazil have been divided into two suites:

(1) A NE main-suite, with (a) and (b) textural types.

(2) A NE sheared-suite, with (c) and intermediate textural types.

3. Chemistry

3.1. Mineral chemistry

Microprobe analyses have been carried out by means of an ARL-SEMQ instrument operating at 15 kV and 20 nA. Representative analyses for pyroxenes and spinels are given in Tables 1 and 2.

Olivines are chemically homogeneous within each sample. Within the nodule population, the compositional range in Fo content is rather narrow: from 89.2 to 92.4.

Orthopyroxenes are unzoned, rarely showing extremely fine exsolution lamellae not resolvable with the microscope. The $Mg/(Fe^{2+} + Fe^{3+})$ ratio in orthopyroxenes (mg_{opx}) correlates positively with the Fo content in olivines ($r_{corr} = 0.91$ for a population of 35 samples). Both parameters are generally believed to be indicative of the residual character of the whole peridotitic assemblage. Because of the small variation range in the Fo content of the olivines, the mg_{opx} has been taken as a variation (depletion) index in the following diagrams. The compositional variation of the orthopyroxenes vs. mg_{opx} is shown in Fig. 2.

Clinopyroxenes have homogeneous core compositions within each sample. Cr-sp exsolution occasionally occurs while opx exsolution is rarer. Two samples (PY3098 and PY3095) carry an appreciable amount of Cr-sp lamellae. They have been estimated by point-counter under reflected light to be below 1.5%. On the basis of this estimate, the pre-exsolved composition of cpx has been calculated (cf. Fig. 3). The compositional variation of clinopyroxenes is shown in Fig. 3.

Spinels are generally unzoned and without appreciable compositional differences among grains within each sample. The Cr/(Cr + Al) ratio shows

TABLE 2

Specimen No.:	1	2	5	7	8	9
Sample:	PY3091	PY3092	PY3101	SA23	CC29	CC37
TiO_2	0.13	0.03	0.08	0.11	0.11	0.15
Al_2O_3	16.26	40.61	35.10	53.56	47.01	58.59
FeO_t	15.85	13.49	13.83	11.40	10.59	10.74
MnO	0.35	0.15	0.16	0.12	0.13	0.11
MgO	14.15	17.90	16.67	19.98	19.64	20.84
Cr_2O_3	52.32	27.54	34.32	15.26	23.35	9.82
SUM	99.06	99.72	100.16	100.07	100.87	100.35
Ti	0.0031	0.0006	0.0017	0.0022	0.0022	0.0029
Al	0.6094	1.3429	1.1871	1.6607	1.4852	1.7736
Fe^{3+}	0.0881	0.0608	0.0400	0.0237	0.0223	0.0240
Fe^{2+}	0.3334	0.2557	0.2917	0.2192	0.2151	0.2067
Mn	0.0094	0.0036	0.0039	0.0027	0.0030	0.0024
Mg	0.6704	0.7483	0.7127	0.7831	0.7844	0.7975
Cr	1.3150	0.6107	0.7783	0.3173	0.4947	0.1993

Representative microprobe analyses of spinels. Cations on the basis of 4 oxygens. Fe^{3+} calculated as in Table 1

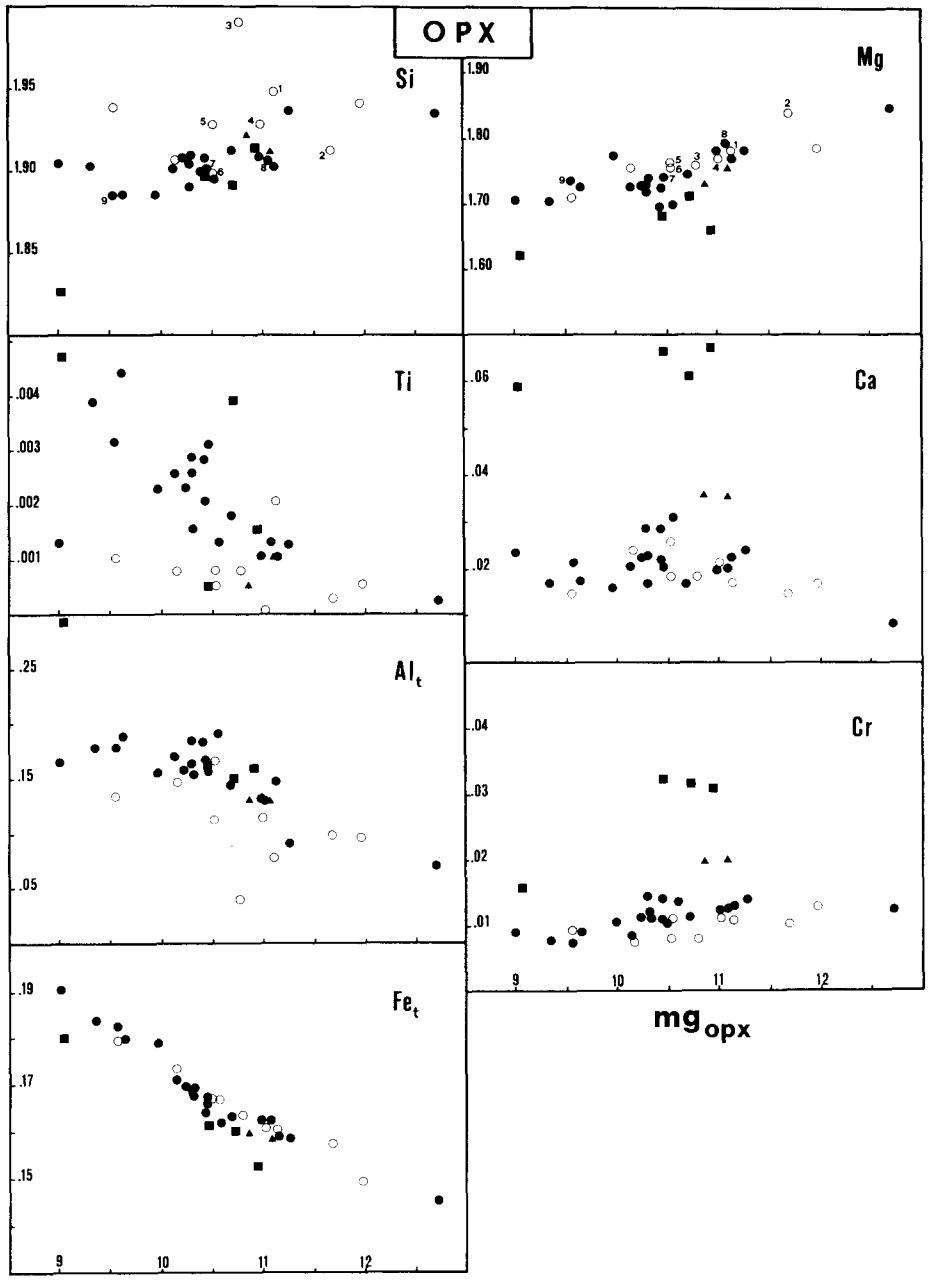

Fig. 2. Compositional variation of the orthopyroxene (cations on the basis of 6 oxygens) vs. the mg_{opx} ($Mg/(Fe^{2+}+Fe^{3+})$ ratio in orthopyroxene. Open circles = PY-suite; black dots = Ne main-suite (samples with coarse-grained and tabular textures); black squares and triangles = NE sheared-suite (samples with porphyroclastic mosaic and intermediate textures, respectively). Numbers correspond to specimen numbers in Table 3.

a large variation range (0.10–0.77) and correlates negatively with the $Mg/(Mg+Fe^{2+})$ ratio, which, however, shows less variation (0.58–0.80). The $Cr/(Cr+Al)$ ratio of the spinels increases with mg_{opx} (Fig. 4) but the nodules richest in blebs (PY3091, PY3093, PY3101) and those belonging to the NE sheared-suite, both characterized by Cr-rich spinels, deviate significantly from the main positive pattern.

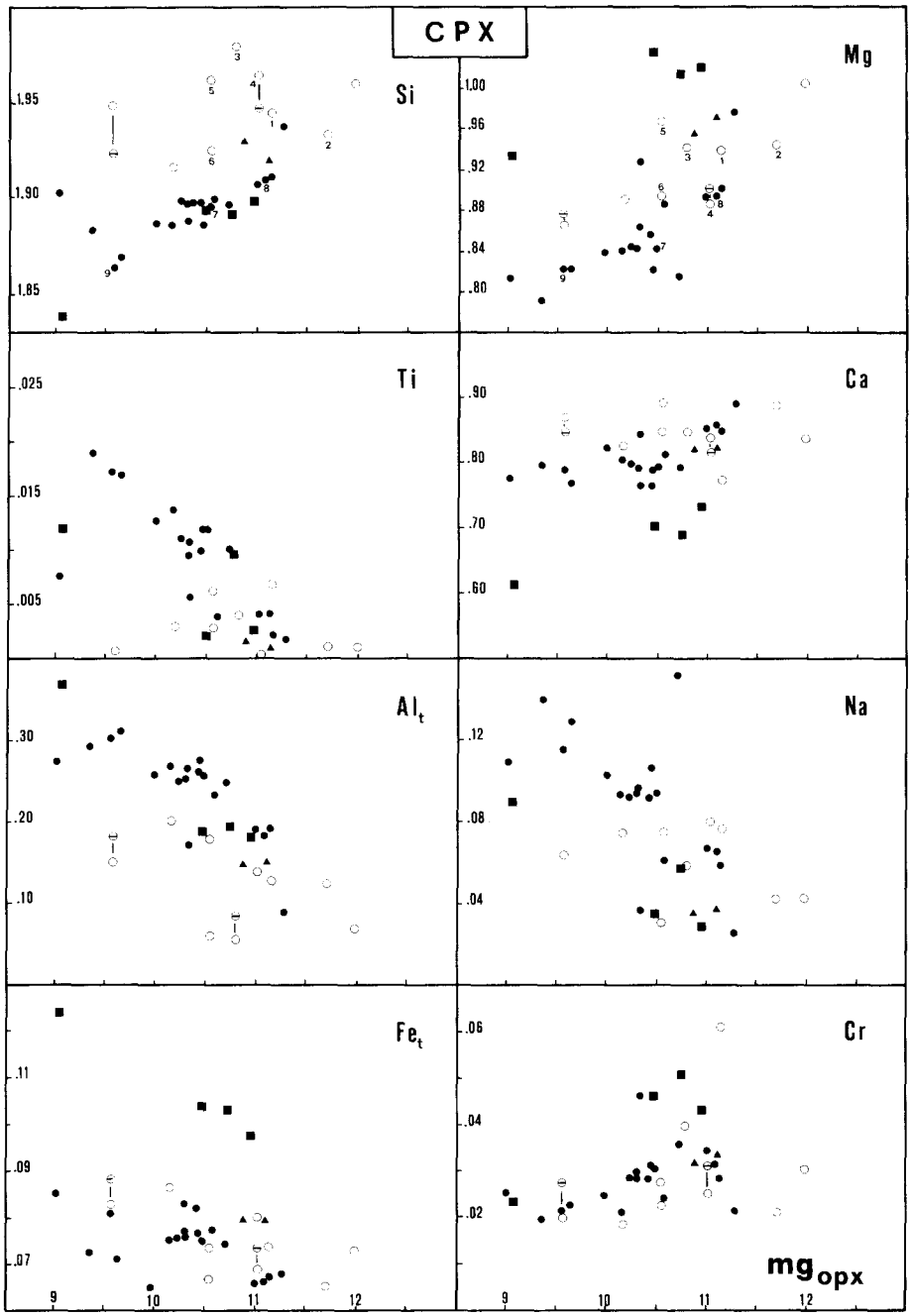

Fig. 3. Compositional variation of the clinopyroxene (cations on the basis of 6 oxygens) vs. the mg_{opx}. Barred circles = calculated clinopyroxene compositions after the addition of 1.5% exsolved spinel. Other symbols as in Fig. 2.

3.2. Bulk chemistry

Nine whole-rock analyses of selected samples with a diameter larger than 7 cm and no lava infiltration have been carried out by XRF methods. For the largest-diameter xenoliths (PY3091, PY3095, CC37: diam. 12 cm), up to 4 aliquots from different portions of each sample have been taken for replicate analyses in order to test the compositional homogeneity. The bleb from sample

TABLE 3

Bulk rock major (wt.%) and trace element (ppm) abundances in 9 selected xenoliths and a bleb. For comparison data obtained on some international standards are reported

Specimen No.:	1		2		3	4		5	6	7	8		9					
Sample:	PY3091		PY3092		PY3093	PY3095		PY3101	PY3103	SA23	CC29		CC37		BLEB	BCR-1	UB-N	NIM-P
n:	4		3		1	3		1	1	1	2		3					
SiO_2	43.08		43.38		42.71	44.48		41.91	44.10	43.53	45.05		44.78		42.61	54.90	39.91	52.58
TiO_2	0.08		0.01		0.10	0.01		0.04	0.04	0.08	0.05		0.15		0.66	2.11	0.10	0.20
Al_2O_3	1.95		0.87		1.42	1.61		1.59	2.18	2.06	1.36		3.28		9.29	14.32	2.11	5.10
FeO_t	8.36		8.01		8.38	7.90		8.78	8.04	8.62	8.40		8.79		6.35	11.49	7.70	10.77
MnO	0.14		0.14		0.14	0.13		0.16	0.14	0.15	0.14		0.15		0.17	0.16	0.12	0.22
MgO	43.23		45.52		44.13	42.62		45.10	41.72	43.04	43.03		38.55		22.54	2.56	36.75	26.10
CaO	1.02		0.88		1.14	1.69		0.71	2.25	1.45	0.92		2.99		5.99	6.70	1.11	3.05
Na_2O	0.43		0.15		0.35	0.19		0.22	0.20	0.01	0.04		0.25		2.35	3.57	0.06	0.37
K_2O	0.59	(0.07)	0.05	(0.03)	0.50	0.40	(0.06)	0.43	0.39	0.07	0.08	(0.03)	0.10	(0.04)	2.93	1.71	0.02	0.11
P_2O_5	0.21		0.00		0.20	0.09		0.06	0.02	0.02	0.01		0.02		0.85	0.40	0.00	0.02
Cr (6)[d]	2710		2754		2218	2948		1817	2795	2493	2579		2967		42837	29	2483	23097
Ni (5)	2376		2450		2393	2282		2522	2233	2261	2408		2095		1041	11	1892	502
Ba (3)	65	(14)	26	(7)	54	45	(6)	38	38	24	24	(1)	45	(27)	454	749	31	46
Ce (4)	59	(7)	[1]		49	7	(3)	14	[4]	[2]	[1]		[3]		167	47	n.d.	n.d.
Sr (4)	175	(41)	15	(2)	108	51	(6)	46	28	13	37	(1)	27	(4)	815	316	12	33
Zr (15)	123	(42)	n.d.		224	n.d.		39	29	[5]	n.d.		278	(121)	1679	185	n.d.	[8]
Rb (2)	12	(3)	[1]		12	3	(2)	12	8	[1]	3	(1)	[1]		49	54	11	14
Y (2)	32	(5)	[2]		37	4	(3)	n.d.	7	n.d.	4	(6)	21	(18)	148	34	n.d.	[2]
S (30)	230	(69)	175	(58)	143	223	(83)	229	205	243	276	(30)	276	(30)	209	347	n.d.	n.d.
mg_{opx}	11.12		11.67		10.76	11.00		10.51	10.51	10.20	11.05		9.53					

PY = samples from the PY-suite; SA, CC = samples from the NE main-suite; *n* = number of aliquots used for replicate analyses; ( )[d] = detection limit in ppm; ( ) = standard deviation; [ ] = indicative of a value $\leqslant$ detection limit, but above background; n.d. = not detected; $mg_{opx} = Mg/(Fe^{2+} + Fe^{3+})$ ratio of orthopyroxene.

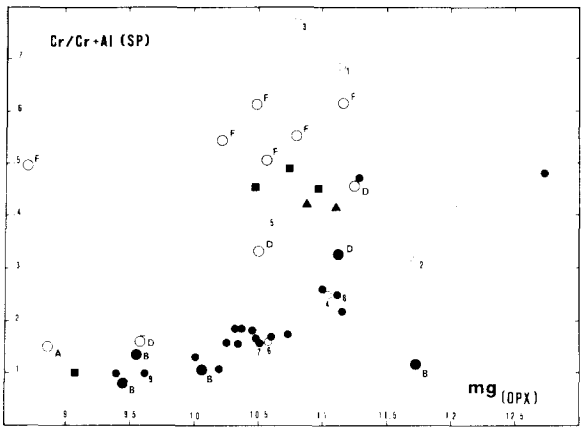

Fig. 4. Cr/(Cr + Al) ratio of spinels vs. the mg_{opx} from PY-suite (small open circles), NE main-suite (small black dots) and NE sheared-suite (black squares and triangles). Numbers as in Fig. 2. Spinels from some hydrous phase or bleb-bearing (large open circles) and anhydrous or bleb-free (large black dots) mantle peridotites are plotted for comparison (see discussion). *F* = alpine peridotite from Finero (unpublished data); *B* = alpine peridotite from Balmuccia [23] and Baldissero [24]; *A* = inclusions from Bullenmerri [25]; *D* = inclusions from Dreiser Weiher [7].

PY3091 was hand picked. The mean values for major and trace elements are given in Table 3. The standard deviation is reported where considered meaningful. Data obtained from some international standards are also reported for comparison.

On the basis of Mg/Si and Al/Si ratios, the selected nodules fit the geochemical fractionation line drawn after Jagoutz et al. [9] (Fig. 5) and outline a depletion sequence ranging from rather primitive (CC37) to strongly depleted (PY3092)

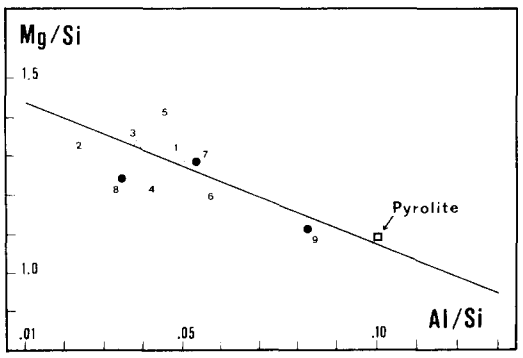

Fig. 5. Mg/Si ratio vs. Al/Si ratio of the selected nodules (open circles = PY-suite; black dots = NE main-suite; numbers as in Fig. 2). The fractionation line and pyrolite composition are reported from Jagoutz et al. [9].

mantle material relative to the pyrolite composition.

As apparent from Table 3, all analysed nodules are K_2O-enriched relative to estimates of primitive mantle compositions ($K_2O = 0.017$ in sample SC1 from [9]; 0.028 [10]; 0.030 [11]). Moreover, the PY samples (except PY3092, which is the only sample of the PY-suite free of blebs or interstitial glassy patches) are anomalously enriched in K_2O and P_2O_5 (perhaps also in Na_2O) even relative to some believed metasomatic mantle peridotites (e.g. $Na_2O = 0.23$, $K_2O = 0.10$, $P_2O_5 = 0.04$ in sample PA10 from S. Carlos [12]; $K_2O = 0.128$ in sample 10051 from Nunivak [13]). High K_2O abundances, similar to those found in PY samples, are only reported in some garnet-peridotite xenoliths (e.g. $K_2O = 0.55$ [14]).

Notably, the PY samples (except PY3092) are distinctive for their very high abundances of incompatible elements, which strongly correlate with their respective contents of K_2O (cf. Table 3).

4. Discussion

4.1 Melting effects on the xenolith population

The compositional variations in bulk chemistry are accompanied by consistent variations in mineral chemistry. With respect to mg_{opx} increase, bulk concentrations of TiO_2, Al_2O_3, CaO, FeO_t decrease and the whole rock compositions become richer in MgO and Ni (cf. Table 3). Correspondingly, the pyroxenes show a depletion pattern in Ti, Al_t, Fe_t, Na and an enrichment in Ca (only for clinopyroxenes), Mg and Si (cf. Figs. 2, 3). Consistently, the coexisting olivines and spinels show more Mg- and Cr-rich compositions respectively (cf. Fig. 4).

The above correlations observed within the NE main-suite and the PY-suite appear to be compatible with effects caused by progressive partial melting process in the spinel peridotite facies.

4.2. Evidence of metasomatic events and origin of the blebs

All bleb-bearing xenoliths are anomalously rich in K and incompatible elements and belong to the PY-suite.

In Table 4 the K/Ba, K/Rb and Ba/sr ratios

of xenoliths, the analysed bleb and the host lavas are listed. The ratios in xenoliths and the bleb are notably different from those in the respective host lavas. In addition to petrographic observations, this fact excludes the possibility that the high abundances of incompatible elements result from host lava contamination. In the same table, ratios relative to mantle-derived hydrous phases [15] are also reported for comparison. The close similarity of these ratios to those of PY samples suggests that amphibole and phlogopite were present in the PY inclusions at some time. A mass-balance calculation has been made in order to obtain the mineralogical composition of the bleb (cf. step 1 in caption of Table 5). The obtained amphibole/phlogopite ratio varies from 0.8 to 1.1 depending on the composition of the hydrous phases used ([16,17], respectively). On this basis, the presence of only one hydrous phase is incapable of accounting for the bleb composition. This fact is apparent from the high contents of both Na_2O and K_2O in Table 3. The present absence of hydrous phases does not invalidate the above conclusion: if the xenoliths were sampled at a relatively high temperature, the large decrease in P_{load} relating to the rapid magma rise, could have produced complete melting of any hydrous phases present.

Incompatible element abundances in the selected xenoliths and the bleb, normalized to incompatible element abundances in primitive mantle [11], are shown in Fig. 6. For comparison, two phlogopite and amphibole-bearing xenoliths from Nunivak [13] are also reported. Quite different abundance patterns are exhibited by the PY and NE (+PY3092) samples.

The PY samples have K contents 10–20 times greater than primitive mantle and are strongly enriched in incompatible elements relative to Nunivak inclusions. They are also characterized by low Ba/K ratios and high Sr contents relative to the NE nodules, a fact which might reflect a larger modal abundance of amphibole compared with phlogopite. As for the high Ce and P_2O_5 (see Table 3) contents in samples PY3091 and PY3093, they should be attributed to the occurrence of pre-existing apatite.

On the basis of the above data and comparisons, the PY nodules are considered to be residual mantle material which has suffered a metasomatic event in very large, but variable, degrees. It is reasonable to suppose that the metasomatic event occurred after the main melting and depletion process (e.g., component B after Frey and Green [16]); however, the possibility that metasomatism was also active before and during the melting stage cannot be excluded. The metasomatic event is believed to have produced the hydrous peridotitic assemblage through the growth of amphibole and

TABLE 4

K/Ba, K/Rb and Ba/Sr ratios in xenoliths, bleb and host lavas. Ratios for mantle-derived amphibole and phlogopite [15] are reported for comparison

Specimen No.	Sample	K/Ba		K/Rb		Ba/Sr	
		nodule	lava	nodule	lava	nodule	lava
1	PY3091	75		408		0.37	
2	PY3092	16		415		1.73	
			14		215		0.98
3	PY3093	77		346		0.50	
4	PY3095	74		1107		0.88	
5	PY3101	94		297		0.83	
			13		245		0.94
6	PY3103	85		405		1.36	
7	SA23	24	20	581	218	1.85	0.90
8	CC29	28		221		0.65	
			22		220		0.99
9	CC37	18		830		1.67	
10	bleb	53		496		0.56	
Amphibole		67		1558		0.73	
Phlogopite		51		286		78	

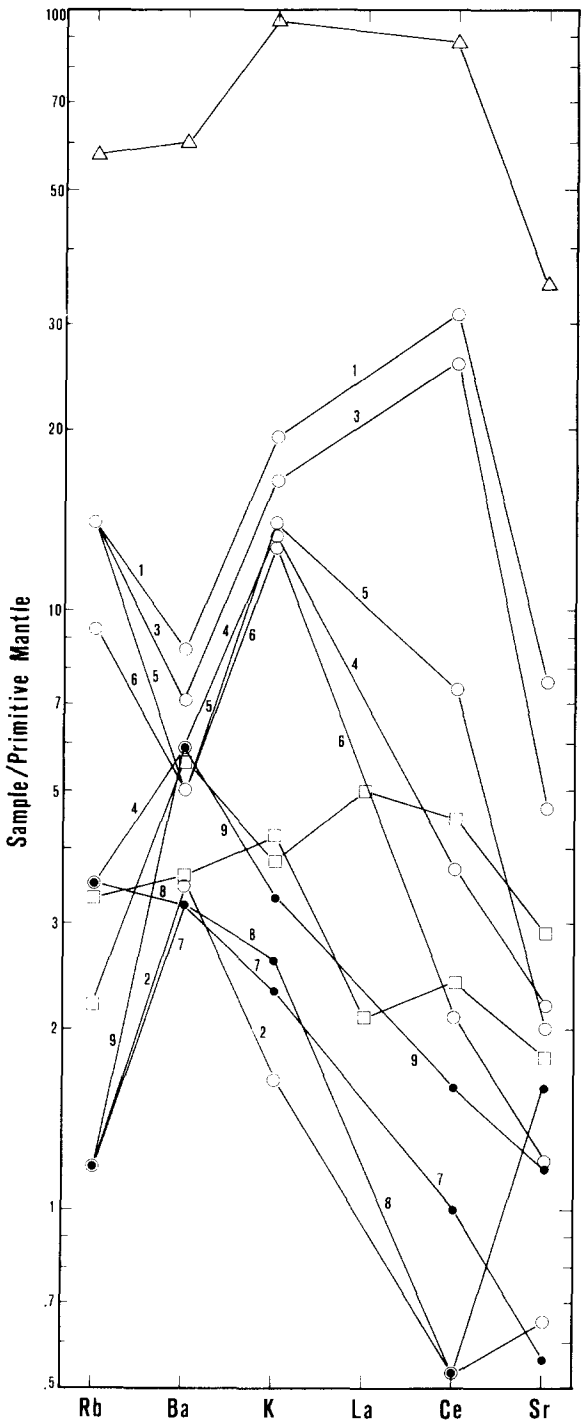

Fig. 6. Trace element abundances in the xenoliths (symbols as in Fig. 5, numbers as in Fig. 2) and bleb (open triangle) normalized to trace element abundances in primitive mantle proposed by Wood et al. [11]. For comparison, also shown are the patterns of amphibole and phlogopite-bearing inclusions (samples 10051, 10075; open squares) from Nunivak [13].

phlogopite crystals. Owing to the incorporation of xenoliths in a rapidly ascending magma, these hydrous phases should represent important loci of local incongruent melting during decompression, resulting in the development of blebs.

Concerning the PY-suite, the hypothesis that the blebs are derived from the melting of hydrous phases is further supported by their textural positions. In PY nodules the blebs always enclose ameboidal relict spinels (Fig. 1a). In many hydrous phase-bearing peridotitic inclusions, amphibole and/or phlogopite generally envelope strongly lobate relict spinels [17]. In the phlogopite-bearing mantle peridotite of Finero (Ivrea-Verbano Basic Complex), which is considered to be a metasomatized mantle slice [18,19], amphibole generally embays a Cr-rich spinel. Such a textural relationship can be explained by the following fluid activity controlled reaction (as proposed by Francis [17]):

$$\text{opx} + \text{cpx} + \text{sp} + \text{fluid} = \text{Cr-amph} + \text{Cr-sp} \qquad (1)$$

The NE (+PY3092) nodules show K abundances 1.5–3 times greater than primitive mantle, and higher Ba/K ratios than the PY ones. On the whole, the concentration patterns of the two

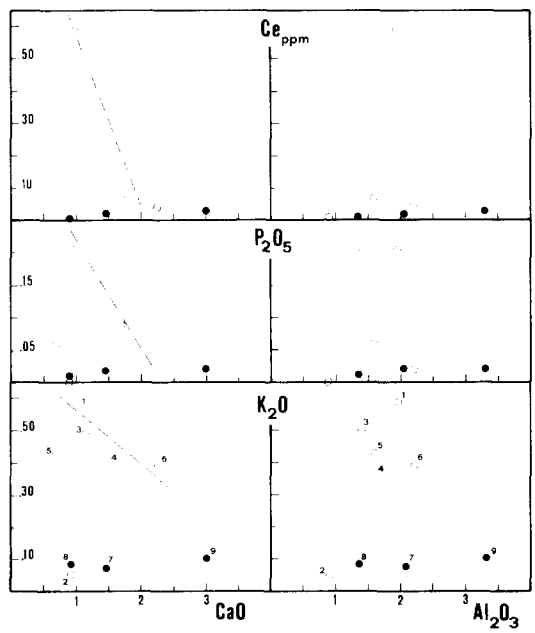

Fig. 7. Bulk contents of some incompatible elements vs. bulk CaO and Al_2O_3 (wt.%). Symbols as in Fig. 5, numbers as in Fig. 2. The best-fit line for PY samples is drawn disregarding samples 2 (PY3092, see text) and 5 (PY3101 which is modally inhomogeneous).

metasomatized inclusions from Nunivak are intermediate between those of the NE- and the PY-suites. Comparing these values to the K and Ba amounts reported in many xenoliths believed to be representative of both undepleted and unmetasomatized mantle [9,13], the abundances of these elements in the NE main-suite (and sample PY3092) are relatively high. Therefore, this suite might also have suffered a metasomatic event, but if so it must have been much less intense than that affecting the PY-suite. The possible metasomatism also appears to have been less intense than that suffered by the amphibole and phlogopite-bearing inclusions from Nunivak, and apparently did not involve the development of hydrous phases. Since no blebs occur in this suite, it can be inferred that if metasomatic event did take place it resulted in an intergranular or pellicular component [20,21].

A frequently observed feature, both in garnet and spinel peridotite facies, is that the most depleted inclusions have the highest K and incompatible element abundances. Frey [22] points out that a decoupling of incompatible elements (K, P, Th, U, LREE) and bulk CaO-Al_2O_3 abundances is found in all peridotite inclusions studied in detail. In Fig. 7, Ce, K_2O and P_2O_5 abundances are plotted vs. CaO and Al_2O_3 bulk contents. The NE (+PY3092) samples are characterized by a nearly steady (or at least slightly increasing) trend. The PY samples show an appreciable negative correlation with increasing CaO and a generalized trend with increasing Al_2O_3. Within the PY-suite, the most metasomatized samples (PY3091, PY3093) carry the lowest clinopyroxene abundances (Table 5).

4.3. Difference in pyroxene and spinel chemistry between the NE main-suite and the PY-suite

The PY-suite is clearly distinguishable from the NE main-suite by its mineral chemistry. First, both the orthopyroxenes and clinopyroxenes of the PY-suite are characterized by higher contents of Si and lower Al_t (resulting from lower contents of both Al^{IV} and Al^{VI}) and Ti. Secondly, appreciable but less marked differences between these two suites can also be seen in the Ca, Mg (and Na) contents of clinopyroxenes (cf. Figs. 2, 3). Relative to mg_{opx}, spinels from the PY-suite are richer in Cr than those from the NE main-suite (cf. Fig. 4), and the PY-nodules generally span a higher mg_{opx} range than the NE nodules.

In order to explain the differences in mineral chemistry between the PY- and NE main-suites, it is suggested that two distinct causes are involved:

(1) Relative to the NE main-suite, the PY-suite on average represents more depleted mantle material. This interpretation is in agreement with the broadly higher mg_{opx} values of the PY-suite and with the variation patterns in the mineral chemistry of the two suites as a whole. However, this does not explain why the PY-suite pyroxenes are richer in Si and poorer in Al_t and Ti than the NE main-suite pyroxenes, and why the spinels are richer in Cr than those of the NE main-suite, in spite of identical mg_{opx}.

TABLE 5

Phase abundances calculated by a least-square program. For the bleb-bearing samples, the calculation has been made in two steps: (1) bleb = opx + cpx + sp + amph + phlog; (2) whole rock = ol + opx + cpx + bleb. a = abundances calculated using amphibole and phlogopite compositions from [16]; b = abundances calculated using the mean compositions of amphiboles and phlogopites from [17]

Specimen No.:	1		2	3		4		5		6		7	8	9
Sample:	PY3091		PY3092	PY3093		PY3095		PY3101		PY3103		SA23	CC29	CC37
	a	b		a	b	a	b	a	b	a	b			
ol	68.8	69.3	72.4	78.7	79.0	65.9	66.1	79.1	79.4	63.4	63.7	70.1	62.9	53.3
opx	18.0	18.1	22.5	10.4	10.4	21.7	21.7	12.8	12.8	21.1	21.1	21.5	32.1	29.7
cpx	2.4	2.5	3.9	3.6	3.7	6.3	6.4	1.1	1.2	8.8	8.8	6.6	3.9	14.8
sp	1.8	1.7	1.2	1.2	1.2	1.0	1.0	1.1	1.1	1.1	1.1	1.8	1.1	2.2
amph	4.0	4.4	–	2.7	3.0	2.3	2.5	2.6	2.9	2.5	2.8	–	–	–
phlog	5.0	4.0	–	3.4	2.7	2.8	2.3	3.3	3.6	3.1	2.5	–	–	–
Σr^2	1.17 [a]		0.37	0.30 [a]		0.32 [a]		0.36 [a]		0.38 [a]		0.49	1.20	1.57

[a] Refers to step 2.

(2) As discussed in the previous section, the compositional differences in the mineral phases between the PY- and NE-suites are accompanied by a sharp difference both in degree and kind of metasomatic effects. Such differences could have resulted from subsolidus re-equilibration with the hydrous phases, and could thus be indirectly related to metasomatism .

In Figs. 8 and 4, the compositions of pyroxenes and spinels from the PY- and NE main-suites are compared with those from other peridotite occurrences [7,23–26]. Whenever the hydrous phases (or blebs) occur in the peridotitic assemblages, for equivalent mg_{opx} values, the pyroxenes are richer in Si and poorer in Al_t and Ti, and the spinels are richer in Cr than those from anhydrous (or bleb-free) peridotitic assemblages. This feature suggests that the growth of amphibole and/or phlogopite during the metasomatic event must affect the pyroxene and spinel chemistry to some extent, as

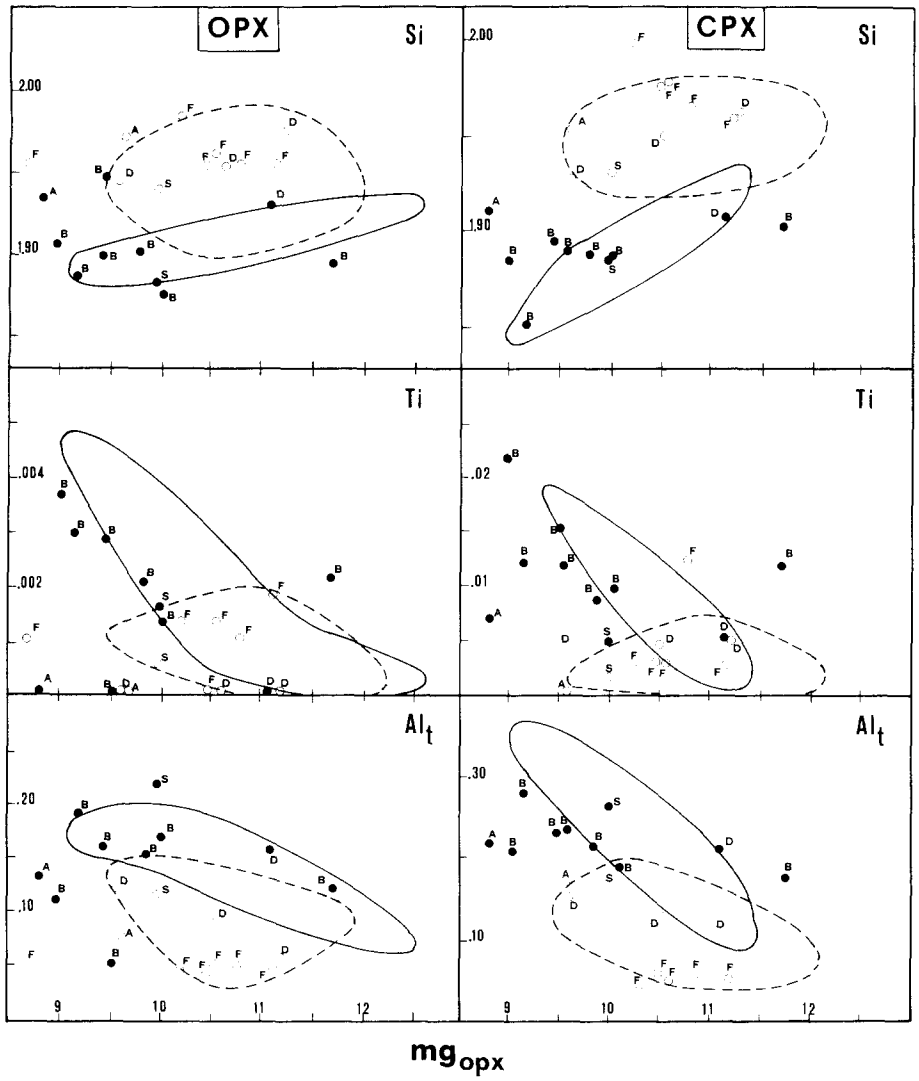

Fig. 8. Compositional variation of the clinopyroxenes and orthopyroxenes vs. mg_{opx}, from mantle peridotites which carry hydrous phases or blebs (open circles) and anhydrous or bleb-free mantle peridotites (black dots). *S* = inclusions from Dreiser Weiher [26]; other letters as in Fig. 4. The pyroxene compositional fields of PY-suite (dashed field) and NE main-suite (enclosed field) are given for comparison.

also suggested by Griffin et al. [25], according to the fluid-controlled reaction (equation (1)). Since the $K_{d\text{amph/px}}^{Al_t/Si}$ is notably larger than the $K_{d\text{amph/px}}^{Fe_t/Mg}$ [16,17,25], the growth of amphibole during the metasomatic event is expected to induce an appreciable decrease in the Al_t/Si ratio of pyroxenes, without substantially affecting their Fe_t/Mg ratio.

If, on one hand, this alternative interpretation explains the different mineral trends of the PY- and NE main-suites relative to mg_{opx}, it does not explain on the other hand why the PY-suite has higher values of mg_{opx} than the NE main-suite. It can, however, be suggested that a more advanced depletion of the PY-suite with respect to the NE main-suite has been overprinted by a re-equilibration of its mineral phases with hydrous phases.

In the variation diagrams of pyroxenes and spinels the NE sheared-suite deviates significantly from the trends outlined by the nodules of the other two suites. It can be seen that: (a) the orthopyroxenes (cf. Fig. 2) display the highest contents of Ca and Cr, and lowest of Mg; (b) the clinopyroxenes (cf. Fig. 3) exhibit the highest contents of Fe_t, Mg, Cr, and the lowest of Ca; (c) spinels are richer in Cr than those from the NE-main suite (cf. Fig. 4).

A combination of similar characteristics in pyroxene chemistry accompanying deformation-recrystallization textures, has been observed in garnet-peridotite xenoliths from kimberlites [27, 28]. However, the NE sheared-suite is at present too poorly represented to make any inferences about such a relationship.

4.4. Sulfur distribution

The interpretation of the sulfur data is constrained by the small size of the xenoliths and by inhomogeneous distribution of the sulfides. Nevertheless, the sulfur content shows a rather clear negative correlation with the variation index mg_{opx} (Fig. 9a), suggesting a direct relationship between sulfur abundances and the residuality of the nodules (in agreement with Garuti et al. [29]). The NE and PY samples outline the same variation pattern (Fig. 9a), but no clear correlation is found between S content and bulk K_2O (Fig. 9b). Thus the sulfur content appears to be unrelated to the main metasomatic event suffered by the two suites. However, S is generally nevertheless believed to be metasomatic in origin [30,31] or to be derived from the injection of an immiscible sulfide melt [32]. If a metasomatic event was in fact responsible for the S contents in the selected inclusions, it must have been added prior to melting.

5. Conclusions

(1) Coarse-grained peridotite inclusions from Paraguay (PY-suite) are characterized by occurrence of blebs, believed to represent the breakdown products of pre-existing hydrous phases (amphibole and phlogopite). Coarse-grained and tabular peridotite inclusions from northeastern Brazil (NE main-suite) in contrast do not carry blebs.

(2) Growth of the hydrous phases is considered to be related to a metasomatic event that strongly affected the PY-suite and produced a marked enrichment in incompatible elements (K, Na, P, Ba, Ce, Rb, Sr, Zr, Y). On the other hand, the NE main-suite is markedly different and may be considered little if at all metasomatized.

(3) Compositions of pyroxenes and spinels from the two suites show different variation trends. The

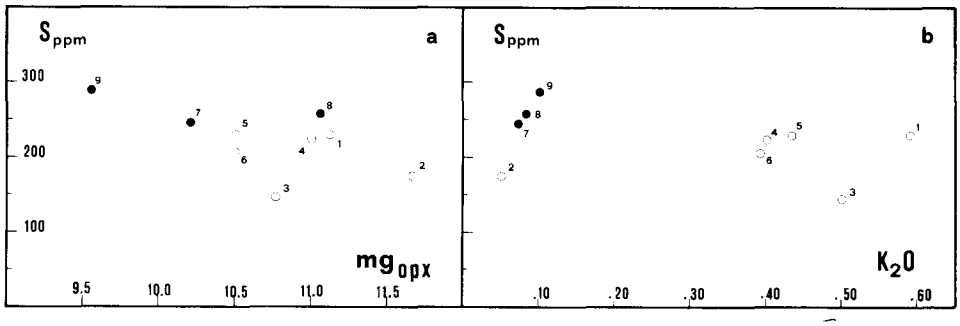

Fig. 9. Bulk S abundances in the selected nodules vs. (a) mg_{opx}, (b) bulk K_2O (wt.%). Symbols as in Fig. 5, numbers as in Fig. 2.

differences are ascribed to the combination of two effects: (a) a more depleted character, on the average, of the PY-suite with respect to the NE main-suite; (b) a re-equilibration of the minerals of the PY-suite with hydrous phases.

(4) Within the PY-suite, a positive correlation seems to exist between the degree of depletion and metasomatism. Such a feature has been already observed in nodule suites from several different localities [22].

In summary, two generalized observations can be made:

(1) On a regional scale, there is a significant mantle heterogeneity: all PY nodules display variable but, on the average, significant metasomatic enrichment in incompatible elements. This feature clearly distinguishes the two suites.

(2) On a local scale there is a limited, but appreciable, mantle heterogeneity. This heterogeneity is testified by the coexistence of nodules with different depletion and metasomatization degree from the same occurrence. The latter type of heterogeneity is common in both peridotitic inclusions and alpine periodites [23,33].

Acknowledgements

The authors have greatly benefited from the critical review and helpful suggestions of Profs. E.M. Piccirillo, G. Rivalenti, G. Ottonello and A. Alberti. The paper was substantially improved also by the critical reading of Prof. K.G. Cox and of an unknown reviewer. The authors are indebted to Prof. A.N. Sial, Dr. C.J. Archanjo and Geol. L.A. Martinez for their field assistance. The C.N.R. is acknowledged for financing the installation and maintenance of the microprobe laboratories at Modena and Milano Universities.

Thanks are due to the Brazilian agencies CNPq, FAPEST and FINEP and to Italian agencies CNR and MPI for financial support.

References

1 C.O. Berbert, D.P. Svisero, A.N. Sial and H.O.A. Meyer, Upper mantle material in the Brazilian shield, Earth Sci. Rev. 17, 109–133, 1981.

2 A.N. Sial, Profundidade de formaçao do magma basaltico terciario do Rio Grande do Norte, deduzida de suas inclusoes peridotiticas, Atas. Simp. Geol. Fortaleza, pp. 173–184, 1975.

3 A.N. Sial, Petrology and mineral chemistry of peridotite nodules included in Tertiary basaltic rock of northeast Brazil, Geol. Soc. Am. Bull. 88, 1173–1176, 1977.

4 A.N. Sial, Chemical behaviour of chromian spinels from ultrabasic nodules included in the Tertiary basalts of Rio Grande do Norte and Paraiba, northeast Brazil, in: 4th Int. Gondwana Symp., Calcutta, p. 90, 1977.

5 J.C. Stormer, J.R.F. Torquato and C.B. Gomes, Age and compositions of nephelinite and enclosed lherzolite nodules from Asuncion, Paraguay, in: 2nd Congr. Latino/Americano Geol., Caracas, pp. 186–187, 1973.

6 J.C. Stormer, C.B. Gomes and J.R.F. Torquato, Spinel-lherzolite nodules in basanite lavas from Asuncion, Paraguay, Rev. Brasileira Geoc. 5, 176–185, 1975.

7 S. Maaløe and I. Prinzlau, Natural partial melting of spinel lherzolite, J. Petrol. 20, 727–741, 1979.

8 A.M. Boullier and A. Nicolas, Texture and fabric of peridotite nodules from kimberlite at Mothae, Thaba Putsoa and Kimberley, in: Lesotho Kimberlites, P.H. Nixon, ed., pp. 57–66, 1973.

9 E. Jagoutz, H. Palme, H. Baddenhausen, K. Blum, M. Cendales, G. Dreibus, B. Spettel, V. Lorenz and H. Wänke, The abundances of major, minor and trace elements in earth's mantle as derived from primitive ultramafic nodules, Proc. 10th Lunar Sci. Conf., pp. 2031–2050, 1979.

10 S.S. Sun, Chemical composition and origin of the earth's primitive mantle, Geochim. Cosmochim. Acta 46, 179–192, 1982.

11 D.A. Wood, J.L. Joron, M. Treuil, M. Norry and J. Tarney, Elemental and Sr isotope variations in basic lavas from Iceland and surrounding ocean floor, Contrib. Mineral. Petrol. 70, 319–339, 1979.

12 F.A. Frey and M. Prinz, Ultramafic inclusions from S. Carlos, Arizona: petrologic and geochemical data bearing on their petrogenesis, Earth Planet. Sci. Lett. 38, 129–176, 1978.

13 M.F. Roden, F.A. Frey and D.M. Francis, An example of consequent mantle metasomatism in peridotite inclusions from Nunivak Island, Alaska, J. Petrol. 25, 546–577, 1984.

14 J. Chen, Petrology and chemistry of garnet lherzolite nodules in kimberlites from South Africa, Am. Mineral. 56, 2098–2110, 1971.

15 W.L. Griffin and V.R. Murthy, Distribution of K, Rb, Sr and Ba in some minerals relevant to basaltic genesis, Geochim. Cosmochim. Acta 33, 1389–1414, 1969.

16 F.A. Frey and D.H. Green, The mineralogy, geochemistry and origin of lherzolite inclusions in Victoria basanites, Geochim. Cosmochim. Acta 38, 1023–1059, 1974.

17 D.M. Francis, The origin of amphibole in lherzolite xenoliths from Nunivak Island, Alaska, J. Petrol. 17, 357–378, 1976.

18 R.A. Exley, J.D. Sills and J.V. Smith, Geochemistry of micas from the Finero spinel-lherzolite, Italian Alps, Contrib. Mineral. Petrol. 81, 59–63, 1982.

19 M. Coltorti and F. Siena, Mantle tectonite and fractionate peridotite at Finero (Italian Western Alps), Neues Jahrb. Mineral. Abh. 149, 225–244, 1984.

20 E. Bonatti, P. Hamlyn and G. Ottonello, Upper mantle beneath a young oceanic rift: peridotites from the island of Zabargad(Red Sea), Geology 9, 474–479, 1981.

21 G. Ottonello, Rare earth abundances and distribution in some spinel peridotite xenoliths from Assab(Ethiopia), Geochim. Cosmochim. Acta 44, 1885–1901, 1980.
22 F.A. Frey, Rare earth elemental abundances in upper mantle rocks, in: Rare Earth Elemental Geochemistry (Development in Geochemistry 2), P. Henderson, ed., pp. 153–203, 1984.
23 P. Comin-Chiaramonti, G. Demarchi, S. Sinigoi and F. Siena, Relazioni tra fusione e deformazione nella peridotite di Balmuccia(Ivrea-Verbano), Rend. Soc. Ital. Mineral. Petrol. 38, 685–700, 1982.
24 S. Sinigoi, P. Comin-Chiaramonti and A. Alberti, Phase relations in the partial melting of the Baldissero spinel lherzolite(Ivrea-Verbano Zone, Western Alps, Italy), Contrib. Mineral. Petrol. 75, 111–121, 1980.
25 W.L. Griffin, S.Y. Wass and J.D. Hollis, Ultramafic xenoliths from Bullenmerri and Gnotuk Maars, Victoria, Australia: petrology of a subcontinental crust-mantle transition, J. Petrol. 25, 53–87, 1984.
26 H.G. Stosch and H.A. Seck, Geochemistry and mineralogy of two spinel peridotite suites from Dreiser Weiher, West Germany, Geochim. Cosmochim. Acta 44, 457–470, 1980.
27 J.J. Gurney and B. Harte, Chemical variations in upper mantle nodules from southern African kimberlites, in: The Evidence for Chemical Heterogeneity in the Earth's Mantle, Philos. Trans. R. Soc. London, Ser. A 297, 273–293, 1980.
28 P.H. Nixon and F.R. Boyd, Petrogenesis of the granular and sheared ultrabasic nodule suite in kimberlites, in: Lesotho Kimberlites, P.H. Nixon, ed., pp. 48–56, 1973.
29 G. Garuti, C. Gorgoni and G.P. Sighinolfi, Sulfide mineralogy and chalcophile and siderophile element abundances in the Ivrea-Verbano mantle peridotites (Western Italian Alps), Earth Planet. Sci. Lett. 70, 69–87, 1984.
30 N.E. MacRae, Silicate glass and sulfides in ultramafic xenoliths, Newer Basalts, Victoria, Australia, Contrib. Mineral. Petrol. 68, 275–280, 1979.
31 B. Harte and J.J. Gurney, Ore mineral and phlogopite mineralization within ultramafic nodules from the Matsoku kimberlite pipe, Lesotho, Carnegie Inst. Washington Yearb. 74, 528–536, 1975.
32 R.H. Mitchell and R.R. Keays, Abundance and distribution of gold, palladium and iridium in some spinel and garnet lherzolites: implications for the nature and origin of precious metal-rich intergranular components in the upper mantle, Geochim. Cosmochim. Acta 45, 2425–2442, 1981.
33 S. Sinigoi, P. Comin-Chiaramonti, G. Demarchi and F. Siena, Differentiation of partial melts in the mantle: evidence from the Balmuccia peridotite, Italy, Contrib. Mineral Petrol. 82, 351–359, 1983.